

Kinetic range spectral features of cross-helicity using MMS

Tulasi N. Parashar, Alexandros Chasapis, Riddhi Bandyopadhyay,
Rohit Chhiber, W. H. Matthaeus, B. Maruca, M. A. Shay
*Bartol Research Institute, Department of Physics and Astronomy,
University of Delaware, Newark, DE 19716, USA*

J. L. Burch
Southwest Research Institute, San Antonio, TX, USA

T. E. Moore, B. L. Giles, and D. J. Gershman
NASA Goddard Space Flight Center, Greenbelt, MD, USA

C. J. Pollock
Denali Scientific, Fairbanks, Alaska, USA

R. B. Torbert
University of New Hampshire, Durham, NH, USA

C. T. Russell and R. J. Strangeway
University of California, Los Angeles, CA, USA

Vadim Roytershteyn
Space Science Institute, Boulder, CO, USA
(Dated: September 7, 2018)

We study spectral features of ion velocity and magnetic field correlations in the solar wind and in the magnetosheath using data from the Magnetospheric Multi-Scale (MMS) spacecraft. High resolution MMS observations enable the study of transition of these correlations between their magnetofluid character at larger scales into the sub-proton kinetic range, previously unstudied in spacecraft data. Cross-helicity, angular alignment and energy partitioning is examined over a suitable range of scales, employing measurements based on the Taylor frozen-in approximation as well as direct two-spacecraft correlation measurements. The results demonstrate signatures of alignment at large scales. As kinetic scales are approached, the alignment between \mathbf{v} and \mathbf{b} is destroyed by demagnetization of protons.

Introduction Turbulence is a ubiquitous feature of astrophysical plasma flows. Interplanetary spacecraft observations have been used to study various aspects of plasma turbulence over the last few decades including the systematic appearance of correlations of several types between fluctuations of the plasma velocity and the fluctuations of the magnetic field (e.g. [1–5] and many references therein). Such correlations are widely regarded as signatures of magnetohydrodynamic (MHD) fluctuations. Here we employ the unique observational capabilities of the Magnetospheric Multi-Scale (MMS) Mission to examine these hitherto inaccessible correlations at kinetic sub-proton scales.

One of the features of MHD turbulence is the conservation of cross helicity [6]. The normalized cross helicity is defined as

$$\sigma_c = \langle |\delta z^+|^2 - |\delta z^-|^2 \rangle / \langle |\delta z^+|^2 + |\delta z^-|^2 \rangle \quad (1)$$

where $\delta z^\pm = \delta \mathbf{b} / \sqrt{\mu_0 m_i n_i} \pm \delta \mathbf{v}_p$; $\delta \mathbf{b}$ is the increment of magnetic field fluctuation $\mathbf{b}(\mathbf{x}) - \mathbf{b}(\mathbf{x} + \mathbf{r})$, written in Alfvén speed units as suggested by this definition, where \mathbf{r} is a lag, n_i is the proton density, and \mathbf{v}_p is the proton fluid velocity fluctuation (mean removed), and the brack-

ets indicate a suitable volume average. σ_c is sensitive to both the relative alignment of the velocity and magnetic fluctuations, and their degree of energy equipartition. For an “Alfvénic” state the magnitude of cross helicity is very close to the value for Alfvén waves (~ 1). A lower value suggests a non-Alfvénic state. The importance of the ideal incompressible invariant cross helicity $\langle |z^+|^2 - |z^-|^2 \rangle$ in selecting equilibria was noted early on by Chandrasekhar [7] and Woltjer [8]. Later, in the context of MHD turbulence theory [9, 10] it was noted that relaxation of energy in both 2 and 3-dimensions can lead to states that tend toward *point-wise* geometrical alignment, but not necessarily equipartition, of \mathbf{v} and \mathbf{b} . Simulations subsequently showed that this tendency occurs rapidly and locally [11–14]. Subsequent research exploited the tendency for alignment of v & b fluctuations to estimate the degree of suppression of nonlinearity, thus influencing the slope of the turbulent spectrum [15–18].

The situation becomes more complex as proton kinetic scales are approached, and non-MHD effects are expected. As the differential flows of protons and electrons become important, the concept of helicity must be generalized [14, 19]. At sub-proton scales, one could an-

anticipate an electron MHD regime. However, in this paper we are interested in scales approaching proton kinetic scales and hence limit ourselves to the definition of σ_c based on center of proton velocity. The generalization of the cross helicity invariant [14] has not been discussed, as far as we know, beyond a Hall MHD description. Even here, as kinetic scales are approached the “frozen-in” approximation breaks down, small plasma parcels are not tied to field lines and may not align with it. Hence it is likely that flow-magnetic field alignment gets significantly modified. However, how the alignment deviates from MHD behavior at kinetic scales has not been studied, to the best of our knowledge.

The residual energy (difference of energy density in flow fluctuations and magnetic fluctuations) is related in MHD to the alignment issue both kinematically and dynamically. The normalized residual energy, $\sigma_r = (\delta\mathbf{v}^2 - \delta\mathbf{b}^2)/(\delta\mathbf{v}^2 + \delta\mathbf{b}^2)$ obeys an exact kinematic relation involving the alignment cosine: $\cos(\theta) \equiv (\delta\mathbf{v} \cdot \delta\mathbf{b})/\sqrt{|\delta\mathbf{v}||\delta\mathbf{b}|} = \sigma_c/\sqrt{1 - \sigma_r^2}$. This relationship holds point-wise and for averages. Even prior to invoking turbulence theory, one sees readily, for a pure non-dispersive Alfvén wave packet, that one necessarily has $\sigma_c = 1$, $\cos(\theta) = \pm 1$, and $\sigma_r = 0$. Various turbulence theories pertain to the behavior of this angle, and to the residual energy, in MHD and in the inertial range [10, 13, 15]. To the best of our knowledge no theory exists that describes alignment in the kinetic range where the MHD approximation breaks down.

Here we use burst-mode data from the MMS spacecraft to provide a novel view of cross helicity, alignment and residual energy in the solar wind as well as the magnetosheath, exploiting MMS time-resolution and the multi-spacecraft observations to probe these quantities in the kinetic range.

Data: We use data from the four spacecraft MMS mission, which emphasizes high cadence observations of magnetic reconnection [20, 21]. The magnetic field data are obtained from the Fluxgate Magnetometer (FGM) [22], providing 128 samples per second. The plasma moments used here are taken from the Fast Plasma Instrument (FPI) [23], providing proton moments at 15 samples per second, and electron moments at 30 samples per second. The four MMS spacecraft maneuver in a tetrahedral formation, varying the inter-spacecraft separation over a wide range of distances. The spacecraft separation during the intervals employed here lies below proton inertial length $d_i = c/\omega_{pi}$, where c is the speed of light and ω_{pi} is the proton plasma frequency. We study two intervals: i) A 40 minute long magnetosheath interval from 2017-12-26 starting at 06 : 12 : 43 UTC and ii) An hour long interval in the solar wind from 2017-11-24 starting at 01 : 10 : 03 UTC.

The solar wind data from FPI instrument was significantly polluted by the spacecraft spin-tones and various measurement artifacts that are more pronounced in the solar wind. The data is cleaned in two steps: • The spin-tones and other spurious signals had distinctive peaks in

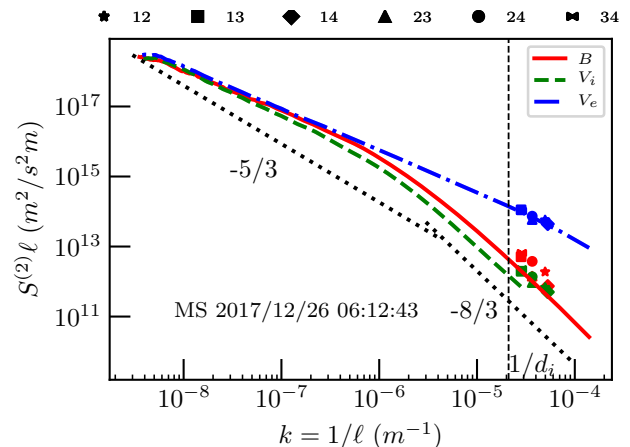


FIG. 1: Magnetosheath case. Equivalent spectra computed from structure functions show the same behavior as the Fourier spectra. The spectra computed using Taylor’s hypothesis from single spacecraft measurements agree very well with the multi-spacecraft estimates well into the kinetic range.

the spectrum. The peaks were identified by the Hampel algorithm and their amplitudes were rescaled to the expected spectral amplitude while keeping the phase information intact. • The resulting time series was then low pass filtered at $1Hz$ to avoid noise associated with the noise floor of the instrument. For details of the cleaning algorithm, see [24].

Results: We begin by studying the spectral features of magnetic field and flows. To leverage the advantages afforded by multi-spacecraft observations we compute the equivalent spectra using the structure function technique as described in [25]. The second-order structure function of a vector (e.g. magnetic field) is defined as

$$D_b^{(2)}(\mathbf{r}) \equiv \langle |\mathbf{b}(\mathbf{x} + \mathbf{r}) - \mathbf{b}(\mathbf{x})|^2 \rangle \quad (2)$$

With this definition of $D_b^{(2)}$, $S^{(2)}(\lambda) \equiv D^{(2)}(\lambda) \cdot \lambda$ behaves as an “equivalent spectrum” as a function of an effective wavenumber $k \equiv 1/\lambda$.

Structure functions from a single spacecraft use the Taylor hypothesis to transform time lags into spatial lags, i.e., $\lambda = V\tau$ where V is the mean flow speed and τ the time lag. Multi-spacecraft observations enable the direct computation of structure function at a particular physical lag λ defined by the spacecraft separation, using time averaging to attain statistical significance. The four MMS spacecraft correspond to six different physical lags without resorting to Taylor’s hypothesis. Given the small separation of the MMS spacecraft, the directly computed two point structure functions can be compared with the single spacecraft Taylor hypothesis results at scales well into the kinetic range.

Figure 1 shows the equivalent spectra for the magnetic field, proton velocity, and electron velocity for the magnetosheath interval of interest. As above, the magnetic field

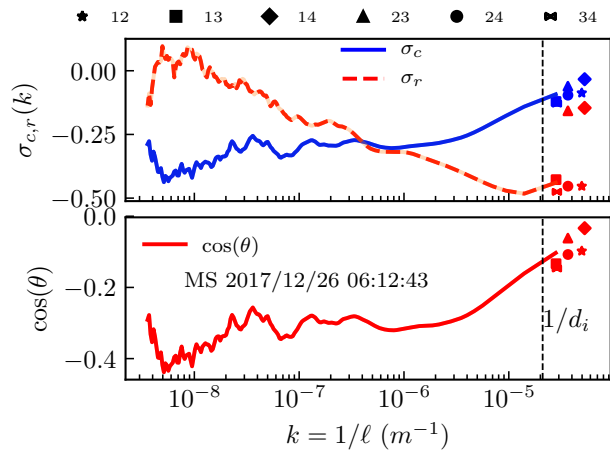


FIG. 2: Magnetosheath case: Equivalent spectrum of cross helicity. Solid line shows the equivalent spectrum from MMS 1, the symbols show multi-spacecraft estimates. The legend at the top specifies symbols corresponding to the spacecraft pairs listed as numbers next to them. At larger scales, the cross helicity is ~ -0.3 and its magnitude decreases as approaching proton kinetic scales and approaches zero deep in the kinetic range.

has been converted to Alfvénic units to make direct comparisons with proton and electron velocities. In the inertial range the magnetic field and the proton and electron velocities have similar power. However, they begin to depart from one another at scales almost a decade larger than d_i . In the kinetic range the multi spacecraft observations match extremely well with the single spacecraft observations computed using Taylor’s hypothesis. This indicates that Taylor’s hypothesis is applicable even in the kinetic range at least to scales slightly below the ion inertial length, consistent with earlier reports [25]. The distances between spacecraft were spread over a moderate range (18.9-35.41 km) and the multi-spacecraft values follow the single spacecraft curve through this range. The slight mismatch of single spacecraft and multi-spacecraft values for protons is likely due to noise in proton measurements.

Having compared the single-spacecraft and multi-spacecraft observations for the familiar spectra of the magnetic field and proton velocity, we now proceed to compute the cross helicity spectrum using the structure function technique described above. First the equivalent spectra of z^\pm are computed and Equation 1 is used to compute the equivalent spectrum of cross helicity.

The top panel of figure 2 shows the equivalent spectrum for cross helicity, computed from the Elsasser variables, for the magnetosheath interval. The figure also shows the estimates of cross helicity at sub-proton lags computed using multi-spacecraft lags. At larger scales the interval has a cross helicity of -0.3 and it approaches 0 as we approach smaller scales. Multi-spacecraft values not only match the single spacecraft estimate, they

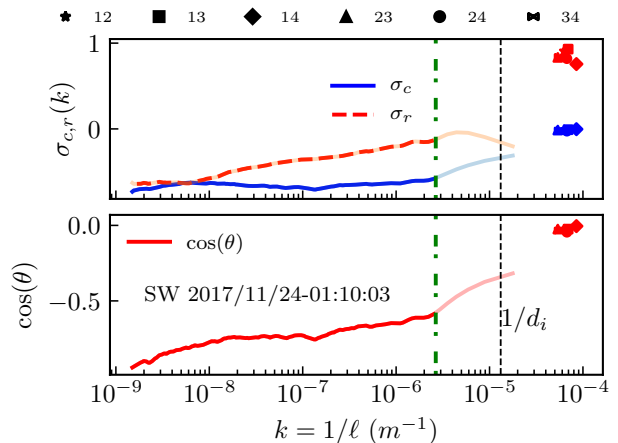


FIG. 3: Solar wind case: Equivalent spectrum of cross helicity. See text for details.

continue the single spacecraft trend. The decrease in cross helicity with decreasing lag indicates that the alignment between flow and magnetic field decreases as kinetic scales are approached. The decrease in cross helicity begins at about the scales where electron and proton spectra depart from each other ($k\ell \sim 10^{-6}$), hence this decrease is likely a direct result of break-down of the MHD approximation. The scales between $k\ell \sim 10^{-6}$ and $kd_i = 1$ are most likely described by Hall-MHD physics, and the generalized helicity [14] would likely be better conserved at these scales. This however requires a computation of vorticity using multi-spacecraft methods, and will be considered in a future study.

The same panel shows the normalized residual energy spectrum for the magnetosheath case. $\sigma_r \sim 0$ at large scales, hinting at near-equipartition of energy between flow and magnetic energies. It decreases approaching smaller scales, indicating a loss in flow energy and dominance of magnetic energy at kinetic scales. Once again, a good agreement with single-spacecraft and multi-spacecraft values is observed. This hints at a difference between magnetosheath and solar wind cases, as will be discussed below.

The bottom panel of this figure shows the alignment angle as a function of scale. At large scales, it has a value ~ -0.4 , indicating a degree of anti-alignment. Approaching kinetic scales, $\cos(\theta)$ approaches zero, indicating a lack of (anti-)alignment. This behavior is also seen for the solar wind intervals that we analyzed.

We turn now to discussion of the spectral features of the selected solar wind interval. Spectra of magnetic field, proton flow and electron flow (not shown) display typical features, e.g. power-law spectra, increasing kurtosis at smaller scales etc.; see Bandyopadhyay et al. [24] for details including issues of cleaning FPI moments in the solar wind. Here we directly move to the study of the equivalent spectrum of cross helicity (shown in figure 3). The vertical green dash-dotted line shows the low-

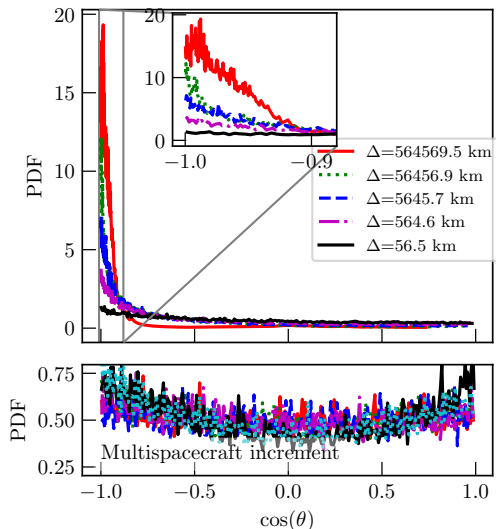


FIG. 4: Solar wind interval: PDFs of alignment angles for various increment lags (top panel) as well as multi-spacecraft lags (bottom panel). Different curves in the bottom panel correspond to different spacecraft pairs. The probability of high degree of alignment decreases for smaller lags. See text for details.

pass scale for the data cleaning procedure [24]. The light blue cross helicity curve extending beyond the low-pass cutoff is the “Fourier interpolated” data, obtained at the original time cadence after imposing the low pass filter. Although the results at these scales show a trend similar to figure 2, the results in this range are of questionable validity.

The cross helicity in figure 3 remains close to -0.7 in the inertial range. As kinetic scales are approached, the cross helicity approaches zero, as was seen in the magnetosheath case. However, because the data at these scales is interpolated, this conclusion is qualitative at best. Nevertheless, this interpretation is further supported by multi-spacecraft measurements of σ_c , that are seen also to be close to zero. The overall qualitative picture is similar to what was observed in the magnetosheath, supporting the idea that the trends seen here are not an artifact of sampling, noise, or the data cleaning procedure.

The residual energy for the solar wind interval, also shown in Figure 3, is magnetically dominated at large scales with a value ~ -0.6 , and, moving towards proton scales, it approaches equipartition. It is interesting that the multi-spacecraft estimates, deep in the sub-proton kinetic range, have values approaching $\sim 1.$, indicating a preponderance of fluctuation flow energy compared to magnetic energy. The alignment angle spectrum shown in bottom panel of figure 3 also supports the “isotropization” conclusion. Evidently the multi-spacecraft data indicate that magnetic and velocity field have little or no preference to be aligned at the 10 km scale, deep in the kinetic range.

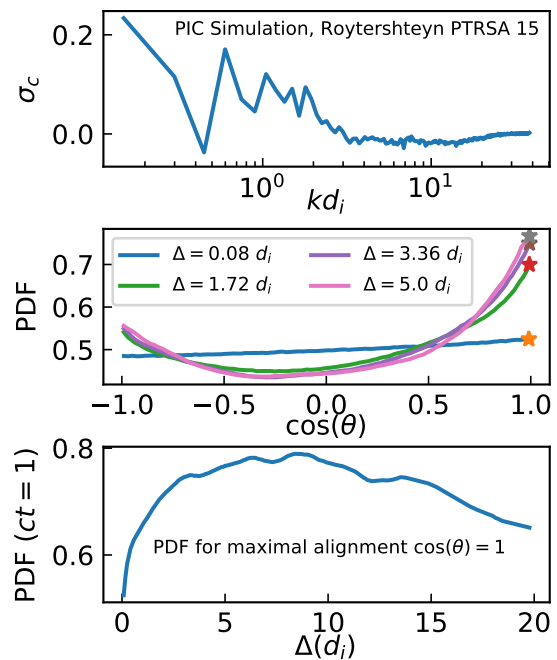


FIG. 5: Cross helicity spectrum, alignment PDFs for small increments, and probability of maximal alignment as a function of lag. See text for details.

Alignment can be further studied by examination of the probability distribution functions (PDFs) of alignment angles, shown in figure 4. The top panel shows PDFs of $\cos(\theta)$ obtained from increments, from single spacecraft measurements and for lags ranging from 56 km to 5.6×10^6 km, that is, from sub-proton scales to several correlation scales. The bottom panel shows PDFs for $\delta \mathbf{v}$, $\delta \mathbf{b}$ alignment cosines computed from multi-spacecraft lags, corresponding to kinetic scale measurements. The inset shows a magnification of the initial part of the PDFs. In this particular interval the alignment PDFs peak at $\cos(\theta) = -1$, consistent with $\sigma_c = -0.7$ at large scales. However, a counter-intuitive result is that decreasing the lag decreases the alignment probability even in the inertial range. Once kinetic scales are approached, the alignment is essentially absent, consistent with demagnetization of the protons. Multi-spacecraft PDFs show very slight departures from isotropy. However, the values are close to 0.5 and the PDFs can be treated as almost isotropic.

Discussion: We have presented an analysis of proton velocity and magnetic field fluctuation correlations, alignment and partitioning of energy, studying the transition from MHD to kinetic scales. Such studies are enabled in the MMS mission by the unique combination of high time cadence and inter-spacecraft separation, in both magnetosheath and solar wind.

Our main observational results, for the selected intervals, are as follows: • The normalized *cross helicity* σ_c tends towards zero for decreasing scale approaching

proton kinetic scales. This has been anticipated in theory [26], but is not always manifest in observations [27] nor realized even in MHD for varying types of turbulence (e.g., [28]). Spacecraft observations of σ_c in the kinetic range have not been previously reported. • The *residual energy* σ_r observed here is consistent with previous theoretical discussions (e.g., [29] and Refs. within.) that argue for vanishing of σ_r at high wavenumber in high Reynolds number MHD. Solar wind observations at MHD scales show a somewhat less clear tendency [30]. • The *alignment angle* also goes to zero towards kinetic scales and into the kinetic range. This is a general phenomenon that we have observed in every interval that we analyzed, which is inconsistent with MHD simulation [10] and MHD theory [15]. Evidently it is a purely kinetic plasma physics phenomenon, deserving of further theoretical study.

Simulation. To further support and elucidate these, we present an analysis from a fully kinetic 3D PIC simulation [31]. The simulation was done on 2048^3 grid points, with $L = 42$. d_i , $\beta_i = \beta_e = 0.5$, with $\sim 2.6 \times 10^{12}$ particles, and an initial cross helicity of ~ 0.44 . The analysis is performed on a snapshot late in time-evolution of the simulation. For more details, refer to [31]. Figure 5 shows the corresponding simulation results for cross helicity, alignment, and residual energy σ_c , to be compared with the main observational results above. The Figure shows that σ_c approaches zero in the kinetic range, consistent with the observations. The PDFs of $\cos(\theta)$ show decreasing probability of pure alignment approaching proton kinetic scales. In the bottom panel we also plot the probability of

maximal alignment (stars in middle panel) as a function of lag. The probability of maximal alignment increases with decreasing lag initially, consistent with MHD theories [12, 13, 15]. However, at around $10 d_i$, the maximal probability begins to drop, indicating increasing frequency of non-aligned proton flow and magnetic field at smaller scales.

These results strengthen the idea that the alignment dynamics are much richer in the kinetic range than they are in inertial range dominated by MHD. The MMS instrument suite opens the doors for these and other novel space plasma studies by providing high resolution plasma measurements in the kinetic range. Data sets with varied parameters and of longer durations are needed to start exploring some of these counter intuitive and “non-MHD” results. Generalizations of cross helicity, EMHD behavior deep in the kinetic range, as well as further implications of these concepts for kinetic range turbulence are topics for future study.

Acknowledgments

This study was supported in part by NASA by the MMS T&M project under grant NNX14AC39G, by LWS program under grant NNX15AB88G, by the Heliophysics Guest Investigator program under grant NNX17AB79G, by NASA grant NNX17AI25G, and by NSF SHINE program under grant AGS-1460130 .

-
- [1] P. J. Coleman, Jr., The Astrophysical Journal **153**, 371 (1968).
- [2] J. W. Belcher and L. Davis Jr., J. Geophys. Res. **76**, 3534 (1971).
- [3] C. Tu and E. Marsch, Space Science Reviews **73**, 1 (1995).
- [4] R. Bruno and V. Carbone, Living Reviews in Solar Physics **10** (2013), URL <http://www.livingreviews.org/lrsp-2013-2>.
- [5] C. H. K. Chen, Journal of Plasma Physics **82**, 535820602 (2016).
- [6] W. Matthaeus and M. Goldstein, Journal of Geophysical Research **87**, 6011 (1982), ISSN 0148-0227.
- [7] S. Chandrasekhar, Proceedings of the National Academy of Science **42**, 273 (1956).
- [8] L. Woltjer, Proc. Nat. Acad. Sci. USA **44**, 833 (1958).
- [9] A. C. Ting, W. H. Matthaeus, and D. Montgomery, Physics of Fluids **29**, 3261 (1986).
- [10] T. Stribling and W. H. Matthaeus, Physics of Fluids B **3**, 1848 (1991).
- [11] L. J. Milano, W. H. Matthaeus, P. Dmitruk, and D. C. Montgomery, Physics of Plasmas **8**, 2673 (2001).
- [12] J. Mason, F. Cattaneo, and S. Boldyrev, Phys. Rev. Lett. **97**, 255002 (2006), URL <http://link.aps.org/doi/10.1103/PhysRevLett.97.255002>.
- [13] W. Matthaeus, A. Pouquet, P. Mininni, P. Dmitruk, and B. Breech, Physical review letters **100**, 085003 (2008).
- [14] S. Servidio, W. H. Matthaeus, and V. Carbone, Physics of Plasmas **15**, 042314 (2008).
- [15] S. Boldyrev, Physical review letters **96**, 115002 (2006).
- [16] J. Podesta, B. D. Chandran, A. Bhattacharjee, D. Roberts, and M. Goldstein, Journal of Geophysical Research: Space Physics **114** (2009).
- [17] J. C. Perez and S. Boldyrev, Physical review letters **102**, 025003 (2009).
- [18] J. Podesta and A. Bhattacharjee, The Astrophysical Journal **718**, 1151 (2010).
- [19] L. Turner, IEEE Trans. Plasma Sci. **PS14**, 849 (1986).
- [20] J. L. Burch, R. B. Torbert, T. D. Phan, L.-J. Chen, T. E. Moore, R. E. Ergun, J. P. Eastwood, D. J. Gershman, P. A. Cassak, M. R. Argall, et al., Science **352** (2016), ISSN 0036-8075, <http://science.sciencemag.org/content/352/6290/aaf2939.full.pdf>, URL <http://science.sciencemag.org/content/352/6290/aaf2939>.
- [21] J. L. Burch, T. E. Moore, R. B. Torbert, and B. L. Giles, Space Science Reviews **199**, 5 (2016), ISSN 1572-9672, URL <https://doi.org/10.1007/s11214-015-0164-9>.
- [22] C. T. Russell, B. J. Anderson, W. Baumjohann, K. R. Bromund, D. Dearborn, D. Fischer, G. Le, H. K. Leinweber, D. Leneman, W. Magnes, et al., Space Science Reviews **199**, 189 (2016), ISSN 1572-9672, URL <https://doi.org/10.1007/s11214-015-0164-9>.

- [//doi.org/10.1007/s11214-014-0057-3](https://doi.org/10.1007/s11214-014-0057-3).
- [23] C. Pollock, T. Moore, A. Jacques, J. Burch, U. Gliese, Y. Saito, T. Omoto, L. Avanov, A. Barrie, V. Coffey, et al., *Space Science Reviews* **199**, 331 (2016), ISSN 1572-9672, URL <https://doi.org/10.1007/s11214-016-0245-4>.
- [24] R. Bandyopadhyay, A. Chasapis, R. Chhiber, T. Parashar, B. Maruca, W. Matthaeus, S. Schwartz, S. Eriksson, O. LeContel, H. Breuillard, et al., arXiv preprint arXiv:1807.06140 (2018).
- [25] A. Chasapis, W. H. Matthaeus, T. N. Parashar, S. A. Fuselier, B. A. Maruca, T. D. Phan, J. L. Burch, T. E. Moore, C. J. Pollock, D. J. Gershman, et al., *The Astrophysical Journal Letters* **844**, L9 (2017), URL <http://stacks.iop.org/2041-8205/844/i=1/a=L9>.
- [26] R. Grappin, A. Pouquet, and J. Léorat, *Astron. Astrophys.* **126**, 51 (1983).
- [27] C.-Y. Tu, E. Marsch, and H. Rosenbauer, *Geophys. Res. Lett.* **17**, 283 (1990).
- [28] W. H. Matthaeus, M. L. Goldstein, and D. C. Montgomery, *Phys. Rev. Lett.* **51**, 1484 (1983).
- [29] R. Grappin, W.-C. Müller, and A. Verdini, *Astron. Astrophys.* **589**, A131 (2016), 1603.03559.
- [30] E. Marsch and C.-Y. Tu, *J. Geophys. Res.* **95**, 8211 (1990).
- [31] V. Roytershteyn, H. Karimabadi, and A. Roberts, *Phil. Trans. R. Soc. A* **373**, 20140151 (2015).